Published in final edited form as:
Dev Biol. 2009 March 15; 327(2): 386–398. doi:10.1016/j.ydbio.2008.12.025.

The Physical State of Fibronectin Matrix Differentially Regulates Morphogenetic Movements *In Vivo*

Tania Rozario[1], **Bette Dzamba**[1], **Gregory F. Weber**[1], **Lance A. Davidson**[2], and **Douglas W. DeSimone**[1,*]

[1]Department of Cell Biology and the Morphogenesis and Regenerative Medicine Institute, University of Virginia, PO Box 800732, School of Medicine, Charlottesville, VA 22908

[2]Department of Bioengineering, University of Pittsburgh, Bioscience Tower 3-5059, 3501 Fifth Avenue, Pittsburgh, PA 15260

Abstract

This study demonstrates that proper spatiotemporal expression and the physical assembly-state of fibronectin (FN) matrix play key roles in the regulation of morphogenetic cell movements *in vivo*. We examine the progressive assembly and 3D fibrillar organization of FN and its role in regulating cell and tissue movements in *Xenopus* embryos. Expression of the 70 kD N-terminal fragment of FN blocks FN fibril assembly at gastrulation but not initial FN binding to integrins at the cell surface. We find that fibrillar FN is necessary to maintain cell polarity through oriented cell division and to promote epiboly, possibly through maintenance of tissue-surface tension. In contrast, FN fibrils are dispensable for convergence and extension movements required for axis elongation. Closure of the migratory mesendodermal mantle was accelerated in the absence of a fibrillar matrix. Thus, the macromolecular assembly of FN matrices may constitute a general regulatory mechanism for coordination of distinct morphogenetic movements.

Keywords

fibronectin; gastrulation; Xenopus; morphogenesis; integrin; matrix assembly; epiboly; polarity; migration; convergent extension

Introduction

A fundamental question in development is whether regulated changes in the physical organization of the ECM can inform both cell fate and morphogenetic decisions *in vivo*. Many multifunctional ECM proteins bind to receptors at cell surfaces and through intermolecular associations, assemble into higher-order structured states such as fibrils, cables and other macromolecular networks. In recent years, it has become increasingly apparent that the architectural state of assembled ECMs may have important functional consequences for the regulation of cell differentiation, cell motility and tissue organization.

*Correspondence: desimone@virginia.edu, voice: 434-924-2172, fax: 434-982-3912.

The relationship between ECM and intracellular processes is one of dynamic reciprocity (Nelson and Bissell, 2006), in which constant feedback reinforces and maintains a cellular microenvironment that is critical to cell, tissue and organ level physiology. ECM confers spatial, physical and biochemical information to cells about their microenvironments (Green and Yamada, 2007). Spatial cues are transduced through the 3D organization of ECM. For example, cell behaviors such as fibroblast migration speed and directionality are enhanced on 3D vs. 2D ECM substrates (Green and Yamada, 2007). Cell fates and morphogenesis are also dependent on the 3D organization of ECM. On 2D substrates, mammary epithelial cells lose their identity, flatten and fail to respond to lactogenic cues. In 3D matrices, they assemble into polarized acinar structures similar to alveoli *in vivo* and secrete milk proteins (Barcellos-Hoff et al., 1989; Lee et al., 1985). Cell fate decisions are also dependent on mechanical properties of the ECM. Human mesenchymal stem cells, grown in the presence of appropriate inductive signals, will differentiate specifically into neurons, myoblasts or osteoblasts when placed on collagen substrates that have been "tuned" to approximate the elastic modulus of brain, muscle and bone tissues, respectively (Engler et al., 2006). In other studies, the differentiation of human mesenchymal stem cells to adipocyte or osteoblast lineages was affected by constraining cell shape using micropatterned ECM substrates (McBeath et al., 2004). These and other *in vitro* approaches highlight the importance of physio-mechanical stimuli from ECM in the control of cell behavior and fate. A significant challenge, however, has been to elucidate whether and how changes in ECM architecture may regulate cell and tissue responses *in vivo*.

Fibronectin (FN) is a multifunctional adhesive glycoprotein of vertebrate ECMs. FN loss-of-function leads to defects in axial extension (Davidson et al., 2006; Marsden and DeSimone, 2003; Yang et al., 1999), polarized cell division (Marsden and DeSimone, 2001), mesoderm specification (George et al., 1993; Georges-Labouesse et al., 1996), and heart development (Trinh and Stainier, 2004). FN is present in at least three distinct physical states in the extracellular compartment: soluble FN dimers, cell-surface bound FN, and FN fibrils. Secreted FN dimers bind initially at cell surfaces to form a pericellular matrix that subsequently can be assembled and remodeled into 3D fibrillar structures (Mosher et al., 1992; Schwarzbauer and Sechler, 1999). In amphibian embryos, FN fibril assembly is spatio-temporally regulated; FN fibrils are assembled on the blastocoel roof (BCR) but not on the blastocoel floor (Boucaut and Darribère, 1983; Davidson et al., 2004; Lee et al., 1984). This spatial localization occurs even though all cells that line the blastocoel cavity are in contact with soluble FN and express integrin α5β1, a FN receptor that has been shown to initiate FN fibril assembly in these and other cells (Fogerty et al., 1990; McDonald et al., 1987). Fibrillogenesis begins at the onset of gastrulation in amphibians and is coincident with a variety of cell and tissue movements at this stage that are known to require FN (Davidson et al., 2006; Marsden and DeSimone, 2001; Marsden and DeSimone, 2003).

A variety of approaches have been used to perturb FN-dependent cell adhesion and signaling at gastrulation in *Xenopus.* Most recently, mAbs directed against FN cell-binding domains (Marsden and DeSimone, 2001; 2003) or the integrin responsible for binding FN (Davidson et al., 2002) were employed along with integrin dominant negative constructs (Marsden and DeSimone, 2003) and morpholino knockdowns (Davidson et al., 2006) to identify the movements and cell fate decisions that involve cell-FN interactions at gastrulation. Each of these studies utilized either acute or chronic functional perturbations to demonstrate that FN-integrin interactions are important for epiboly, convergent extension and mesendoderm migration. However, once FN is expressed *in vivo* it undergoes a progressive process of assembly from surface-bound dimeric to fibrillar, coincident in space and time with the dramatic morphogenetic and signaling events of gastrulation. Whether or not these different organizational states of FN assembly are functionally equivalent has not been addressed by loss-of-function experiments in *Xenopus* or any other developmental system.

Does the 3D architecture of fibrillar FN matrix influence polarized cell movements that are crucial to gastrulation? To investigate functional differences between fibrillar and non-fibrillar states of FN in this system, we expressed the 70 kD N-terminal fragment of FN in embryos in order to interfere with FN-FN interactions important for fibril assembly (McDonald et al., 1987; McKeown-Longo and Mosher, 1985) but not FN-dimer binding to integrins. This method permits integrin binding to the Arg-Gly-Asp (RGD) containing central-cell-binding domain of FN, thus maintaining endogenous FN in a surface-bound pericellular state.

Materials and methods

Embryos and antibody staining

Embryos were obtained and cultured using standard methods and staged according to Nieuwkoop and Faber (Nieuwkoop and Faber, 1994). Keller sandwiches were made from stage 10 embryos as described by Keller and Danilchik (Keller and Danilchik, 1988) and cultured for 6 hours in DFA (Davidson et al., 2002) before fixation. Immunostaining was carried out as described previously (Marsden and DeSimone, 2001; Marsden and DeSimone, 2003) using the following antibodies: mouse anti-FN mAb directed against Type III_{10} repeat of FN (4H2) 1:300; rabbit anti-FN polyclonal Ab (32FJ) 1:2000; rabbit anti-C-Cadherin (Xcad) 1:2000; and mouse anti-α tubulin 1:1000, followed by goat anti-mouse and rabbit IgG conjugated to Alexa-488, -555 or -647 fluorophores. BCRs were mounted in 50% glycerol/PBS on glass slides. Bisected embryos and Keller sandwiches were dehydrated in methanol and cleared in BB:BA (benzyl alcohol, benzyl benzoate) for microscopy.

RNA constructs and microinjection schemes

X. laevis 70 kD FN was PCR amplified from cDNA pD8 (DeSimone et al., 1992) and cloned into the pCS2+MT vector. For the control construct, the first 1.2 kbp was excised by restriction digest with SacI and religated. RNAs were transcribed *in vitro* using SP6 RNA polymerase. Control and 70 kD FN transcripts were injected in 5 nl containing ~1–3 ng of RNA.

Western Blot

Xenopus embryos were solubilized in 200 μL lysis buffer (100 mM NaCl, 50 mM Tris-HCL pH 8.0, 1% Triton X-100, 2 mM PMSF [phenylmethylsulphonylfluoride], 2 μL protease inhibitor cocktail [Sigma P2714]). Protein extracts were diluted in 2X reduced Laemli buffer (2% β-mercaptoethanol), separated by SDS-PAGE (6 or 7%) and blotted onto nitrocellulose for probing with antibodies.

DOC insolubility assay

10 embryos were solubilized in DOC buffer (2% DOC, 1 mM EDTA, 20 mM Tris-HCl pH 8.8, 2 mM Iodoacetic acid and Sigma protease inhibitor cocktail). DOC soluble extract was obtained after centrifugation at 14 K G for 30 min. The DOC insoluble pellet was dissolved in SDS buffer (substitute 2% DOC with 1% SDS). 5% of the DOC soluble extract and 100% of the DOC insoluble extract were analyzed by Western blot and probed with anti-FN mAb 4H2.

Mesendodermal mantle closure

Embryos were pre-fixed in MEMFA (3.7% formaldehyde, 0.1 M MOPS pH 7.4, 2 mM EGTA, 1 mM $MgSO_4$), dehydrated in methanol and rehydrated in PBST (PBS/0.1% Tween). The BCRs were peeled back using forceps and the mesendodermal mantle was imaged using a Zeiss LumarV12 stereomicroscope and Zeiss AxioCam MRm camera. Morphometric measurements were made using AxioVision software.

Mesendoderm migration assay

Glass coverslips were alkaline-ethanol washed and flamed prior to coating with FN. Coverslips were coated with 200 μl of 1–15 μg/ml bovine plasma FN (Calbiochem) overnight at 4° C to yield a maximum coating density of 0.15–2.26 μg/cm2. Mesendoderm tissue was excised from stage 10 Xenopus embryos and placed in Ca^{2+}/Mg^{2+}-free 1X MBS (1X MBS: 88 mM NaCl, 1 mM KCl, 0.7 mM $CaCl_2$, 1 mM $MgSO_4$, 5 mM HEPES pH 7.8, 2.5 mM $NaHCO_3$) to dissociate the tissue to single cells. Cells were then transferred into 1X MBS containing Ca^{2+}/Mg^{2+} on FN-coated coverslips. Cells were allowed to attach for 1 hour, then time-lapse phase-contrast images were acquired for approximately 1 hour using a Hamamatsu Orca camera mounted on a Zeiss Axiovert 35 microscope equipped with a motorized stage driven by OpenLab software (Improvision). OpenLab image files were imported into ImageJ software (NIH) for analysis. Sobel edge detection kernels were used to create an outline defining the perimeter of each cell, and thresholds were set to select individual cells. The centroid of each cell area was tracked over time to determine total cell path length, which was then divided by the total time to calculate average cell speed. Only mesendoderm cells that were attached and spread at the beginning of image acquisition were analyzed for migration speed.

Quantification of FN by Ab binding to live BCRs

Live BCRs were dissected, cultured in ¼ X MBS and incubated in anti-FN mAb 4H2 or anti-Fak mAb 2A7 for 30 min. Caps were then washed, solubilized in lysis buffer (non-reduced) and analyzed by Western blot. Blots were probed for IgG using anti-mouse secondary antibody.

Whole-mount *in situ* hybridization

In situ hybridizations were performed with slight modifications from the standard protocol (Harland, 1991). Protease K digestion was omitted and antisense RNA probes were incubated with embryos for 2 days at 65° C. After staining, the embryos were bleached in 1% H_2O_2/5% formamide/0.5X SSC (Mayor et al., 1995). The cDNA template for Chordin was generously provided by E.M. DeRobertis. To measure the width of Chordin staining, the average of three measurements from anterior, middle and posterior regions of the stained domain were calculated.

Microscopy and Image Analysis

Embryos and explants were photographed on a Zeiss Stemi SV6 stereomicroscope using a Canon G5 color camera. Widefield fluorescent images were collected using a Zeiss Plan-Apo/63X/1.40 objective, Zeiss Axiophot, CoolSnap fx camera and OpenLab software (Improvision). Confocal images were taken on a Nikon C1 confocal microscope with either Nikon/S Fluor/10X/0.50 or Nikon/Plan-Apo/60X/1.40 objectives. 3D image analysis was performed using Volocity software (Improvision).

Results

Exogenous expression of the 70 kD N-terminal domain of FN was used to inhibit FN fibrillogenesis by acting as a competitive inhibitor of the N-terminal matrix assembly domains of the protein (McDonald et al., 1987; McKeown-Longo and Mosher, 1985). We executed this strategy by microinjecting RNA transcripts encoding *Xenopus laevis* 70 kD FN (Fig. 1A) into embryos. Unless stated otherwise, RNA was injected into both blastomeres at 2-cell stage to ensure broad expression of the construct. A non-secreted N-terminal truncation of 70 kD FN (Fig. 1A) was used as a control construct. Both were tagged with 6-Myc repeats. FN assembly can be blocked using other methods including dominant negative inhibition of β1 integrins, FN-integrin function-blocking antibodies, and gene-targeting or morpholino based loss-of-function analyses (Davidson et al., 2006; George et al., 1993; Marsden and DeSimone,

2003). However, each of these methods also abrogates FN-binding to integrins and syndecans at the cell surface and, therefore, may perturb cell signals normally activated following FN adhesion. In contrast, expression of 70 kD FN, inhibits fibrillogenesis without preventing the initial binding of FN dimers to integrins at cell surfaces (Fig. 1B). Thus, 70 kD FN blocks N-terminal associations of FN dimers that are required to assemble a fibril without affecting cell surface interactions with other regions of FN. This allowed us to compare and contrast the contributions of the physical assembly state of FN with the loss-of-function results obtained in earlier studies.

BCRs were dissected and immunostained for FN to confirm that 70 kD FN expression successfully inhibited fibrillogenesis. At mid-gastrula stages, uninjected (UN) and control-construct injected (Con) embryos elaborated extensive fibrillar networks of FN (Fig. 2A–B). Injection of the 40 kD FN control construct caused a short developmental delay which is evident in Fig. 2B where the fibrillar matrix is less dense. With time (~30 min), these embryos assemble dense networks of FN fibrils indistinguishable from uninjected controls. In contrast, 70 kD FN embryos expressed FN in a pericellular arrangement and lacked clearly defined fibrils (Fig. 2C). FN staining was apparent at cell borders in projected Z-stacks (Fig. 2C) and as fine puncta at free cell surfaces facing the blastocoel (not shown). Thus, expression of 70 kD FN successfully blocked fibrillogenesis in our system. Interestingly, cell shapes in BCR tissue were also affected by 70 kD FN expression. Immunostaining with a C-cadherin antibody demonstrated that cells are normally arranged in a polygonal array in the BCR at this stage (Fig. 2D–E). 70 kD FN expression caused BCR cells to become more rounded and disorganized (Fig. 2F) suggesting that cell-cell adhesion was reduced.

The 70 kD FN fragment did not perturb the expression or secretion of endogenous FN. Western blot analysis of total FN levels at gastrula stages showed that levels of endogenous FN were comparable in whole embryos expressing 70 kD FN (Fig. 2G). In addition, we extracted blastocoel fluid from embryos using a glass pipette and found that FN levels in the blastocoel were also unaffected by the expression of 70 kD FN. As expected, 70 kD FN-Myc was present in the blastocoel fluid but the 40 kD FN-Myc control construct was not secreted into the blastocoel because it lacks an N-terminal signal sequence. We attempted to quantify the proportion of endogenous FN assembled into fibrils along the BCR using deoxycholate (DOC) insolubility (McKeown-Longo and Mosher, 1983) but this method was unsuccessful in distinguishing FN fibrils at these stages. While DOC insoluble FN was detected later in development, all FN assembled on the BCR at gastrula stages was sensitive to DOC extraction (Fig. 2H) in both control and 70 kD FN embryos (Fig. 2I).

Because 70 kD FN prevents the assembly of FN fibrils, it is possible that less FN accumulates along the BCR as gastrulation progresses in 70 kD embryos. Therefore, phenotypes observed in the presence of 70 kD may be attributed to changes not only in the 3D-architecture of the matrix but also the number and density of biologically active binding sites in FN. One way to address the possibility that the fibrillar state of FN affects the availability of functionally important sites such as the Arg-Gly-Asp (RGD) containing central-cell binding domain of FN (CCBD; i.e., the binding site for $\alpha 5\beta 1$ and other integrins) is to analyze the binding of domain-specific mAbs in the presence or absence of 70 kD FN. The anti-FN mAb 4H2 recognizes the CCBD of FN (Ramos and DeSimone, 1996). mAb 4H2 was incubated with live control and 70 kD FN BCRs obtained from embryos at early and late gastrula stages. After thorough washing, treated BCRs were solubilized and analyzed by Western blot using anti-mouse IgG to quantify the amount of mAb 4H2 bound to BCR cell surfaces. This assay provides an indirect measure of CCBD binding sites available to cells (e.g., mesendoderm) that come in contact with the BCR.

At early stages of fibrillogenesis (stg. 10–10.5), 4H2 binding to control and 70 kD FN embryos was comparable (Fig. 3). However, as fibrillogenesis progressed with time in normal embryos, 70 kD FN BCRs bound approximately 70% less mAb 4H2 than control BCRs (Fig. 3A–B). Thus, one consequence of normal FN-FN assembly into fibrils is that over time, more total FN is incorporated into a given area of the BCR. This local increase in FN density effectively increases the number and concentration of integrin binding sites that are available to migratory mesendoderm and BCR cells.

Inhibition of FN fibril assembly delays blastopore closure and blocks epiboly at gastrulation but not axial extension

Gastrulation was disrupted when 70 kD FN was broadly expressed in embryos. Nearly all (98%) of the 70 kD FN embryos were stalled relative to controls at gastrulation (Table 1, Fig. 4A–B) until the initiation of a putative second blastopore lip, which preceded blastopore closure (Fig. 4C, red arrowhead). Blastopore closure was delayed by approximately 3 hours at room temperature. By tailbud stage, 73% of the 70 kD FN embryos completed blastopore closure but had shortened anterior-posterior (A-P) axes while 26% failed to complete gastrulation (Table 1, Fig. 4E). Blastopore closure is a complex process that involves a variety of different morphogenetic movements that includes mesoderm involution, convergent extension in the dorsal marginal zone (DMZ), convergent thickening at the periphery of the blastopore and radial intercalation in the BCR (Keller and Shook, 2008;Keller, 1978;Keller, 1980). A defect in one or more of these cell behaviors could result in defective blastopore closure.

In addition to its involvement in blastopore closure, the process of convergent extension is a key morphogenetic process that drives axis elongation in many metazoan embryos (Keller, 2006). During *Xenopus* gastrulation cells in the non-involuting DMZ align mediolaterally and intercalate to drive midline convergence and axial extension (Keller et al., 2000; Shih and Keller, 1992). Because we observed an A-P axis defect in 70 kD FN embryos, we investigated whether convergent extension was compromised. Expression of 70 kD FN was targeted to the DMZ where mediolateral cell intercalation movements are most active, by selective microinjection of transcript into the marginal region of the two presumptive dorsal blastomeres at the 4-cell stage. The dispersion of the 70 kD FN construct was somewhat variable from embryo to embryo but generally confined to the dorsal region that undergoes convergent extension (data not shown). Surprisingly, these embryos extended normally in comparison to the lengths of tailbud stage control embryos (Fig. 4D, F). In contrast, when 70 kD FN was expressed widely in embryos (i.e., by injecting both blastomeres at the 2-cell stage) axial extension was reduced (Fig. 4E,G). This suggests that the source of the axial defect seen in Fig. 4E is not the failure of cells in the DMZ to undergo mediolateral cell intercalation but is a secondary consequence of the failure of one or more other morphogenetic events such as epiboly.

We utilized markers of early dorsal mesoderm to establish whether the patterning or morphogenesis of the DMZ was likely affected by expression of 70 kD FN. As observed in previous studies involving perturbation of FNs or integrins with antibody or morpholino approaches (Marsden and DeSimone, 2003; Davidson et al., 2006) dorsal mesodermal markers were expressed in 70 kD FN embryos. When 70 kD FN expression was targeted to the DMZ, the width of the axial mesoderm marker chordin was comparable to controls (Fig. 4H, I, L) suggesting that convergent extension was not disrupted in the absence of FN fibrils. When 70 kD FN was expressed broadly throughout, two general phenotypes were observed in addition to a general delay in blastopore closure. By stage 13 the majority of these embryos (~70%) had completed blastopore closure and chordin expression was similar to controls (Fig. 4K). The remaining time-matched embryos (~30%) had not completed blastopore closure and chordin was expressed around the dorsal rim of the blastopore and in a broader field of cells

(Fig. 4J). Thus, expression of 70 kD FN in DMZ tissues resulted in normal patterning and extension of axial mesoderm whereas broad expression of 70 kD FN led to longer delays in blastopore closure and defects in extension but did not disrupt patterning. This suggested that movements other than convergent extension might be involved in blastopore closure and mesoderm involution and extension. The mesodermal marker Xbra was also expressed in a similar pattern in 70 kD FN embryos (data not shown). These data concur with earlier studies showing that neither FN nor integrin loss-of-function experiments affected mesodermal patterning (Davidson et al., 2006; Marsden and DeSimone, 2003; Yang et al., 1999).

Convergent extension proceeds in the absence of FN fibrils

The embryo phenotypes resulting from 70 kD expression in the DMZ suggested that convergent extension and axial elongation proceeded in the absence of FN fibrils. This was a surprising conclusion based on a variety of earlier studies involving morpholino knockdowns of FN, expression of dominant negative β1 integrins, and antibody perturbations of integrin and FN adhesion, each of which were shown to inhibit convergent extension and other gastrulation movements (Davidson et al., 2006; Marsden and DeSimone, 2003; Yang et al., 1999). However, in each of these studies, FN binding to cell surfaces was blocked and, thus, the initial pericellular non-fibrillar FN matrix was absent. To confirm whether non-fibrillar FN matrix was sufficient to support convergent extension, we prepared Keller sandwich explants from control and 70 kD FN embryos. When two DMZ explants are sandwiched together, they extend along the A-P axis and form a notochord flanked by presomitic mesoderm (Keller and Danilchik, 1988). We found that 70 kD FN expression had no obvious effect on convergent extension in Keller sandwiches (Fig. 5A–B). Control explants underwent extensive FN fibrillogenesis; a thick mat of fibrillar FN outlined the presomitic mesoderm and fibrils were partially cleared from the dorsal and ventral surfaces of the notochord (Fig. 5C, E) as described previously (Davidson et al., 2004). In 70 kD FN explants, non-fibrillar FN outlined cell boundaries of the presomitic mesoderm and to a lesser extent the notochord (Fig. 5D, G) but no discernable FN fibrils were assembled (what may appear fibrillar in the z-stack projection shown in Fig. 5D is FN localized to cell boundaries, unlike the fibrils that are clearly assembled across cell surfaces in panel 5C). Through-focus z-series and 3D-renderings of 70 kD FN explants confirm the lack of FN fibrils (Fig. 5E, G; supplementary Movies 1 and 2). Despite the absence of fibrils, cells in 70 kD FN explants were elongate and oriented along the mediolateral axis similar to controls (Fig. 5F, H). To confirm that the Keller sandwich data were representative of events occurring *in vivo*, we also bisected late-stage gastrulae (late stg. 12) through the neural plate region (Fig. 5J) to observe notochord-presomitic mesoderm morphology. No obvious morphologic defects were visible between uninjected and 70 kD FN in intact embryos (Fig. 5I, K), which agrees with the explant results. 3D reconstructions of immunostained embryos were also analyzed to confirm that fibril assembly was perturbed in whole embryos expressing 70 kD FN (data not shown).

FN fibrils are required for oriented cell division, BCR thinning and epiboly

Because 70 kD FN expression does not prevent convergent extension, what is the source of the observed gastrulation defects? Based on the results of earlier studies with blocking mAbs (Marsden and DeSimone, 2001) we suspected that epiboly was compromised in 70 kD FN embryos due to failure of radial intercalation and normal thinning of the BCR. In normal gastrulae, radial cell intercalation movements of deep BCR cells cause this 5–6 cell thick tissue to thin to 2-cell layers. This process drives epiboly and encloses the embryo in a thinned sheet of ectoderm (Keller, 1980; Marsden and DeSimone, 2001).

To investigate whether radial intercalation was inhibited in the absence of FN fibrils, the vitelline membranes of early gastrulae (at stg. 10–10.5) were removed and the embryos allowed to develop further. This was done because the vitelline membrane helps maintain the spherical

shape of the embryo at these stages but defects in BCR thinning are less apparent, particularly when other movements (e.g., convergent extension) may be contributing to the epibolic spreading of superficial layers. Without the vitelline membrane, obvious defects in epiboly are observed. As in the case of embryos with intact vitelline membranes, the blastopores of devitellinized 70 kD FN embryos were consistently larger than controls throughout gastrulation (Fig. 6A–B). Devitellinized control embryos completed blastopore closure and were spherical (Fig. 6C) but 70 kD FN embryos were elongate and mushroom shaped (Fig. 6D) with extruded yolk plugs. The animal pole ectoderm of these embryos was bumpy and wrinkled (Fig. 6E) indicating a likely problem with BCR thinning. However, devitellinized 70 kD FN exogastrulae still elongated (not shown), again suggesting that cell behaviors required for axial extension proceeded in the absence of FN fibrils in agreement with our earlier conclusions (Figs. 4 and 5).

Confocal microscopy of bisected gastrulae confirmed that embryos expressing 70 kD FN had enlarged blastocoels and pronounced thickening of the BCR (Fig. 6F–K). This defect was similar to the failure of BCR thinning observed in FN loss-of-function experiments (Marsden and DeSimone, 2001; Marsden and DeSimone, 2003). We also reported previously that function blocking anti-FN mAbs resulted in randomization of mitotic spindle orientation in the BCR (Marsden and DeSimone, 2001), which is normally parallel to the horizontal plane of the BCR (Fig. 6L–M, yellow arrows). A similar randomization of mitotic spindles was observed in embryos expressing 70 kD FN resulting in the accumulation of daughter cells in the vertical plane of the BCR ectoderm in addition to the horizontal plane (Fig. 6N, yellow arrowhead; 6O). Thus, 70 kD FN mediated inhibition of fibril assembly is alone sufficient to abrogate normal spindle orientation and BCR thinning even though non-fibrillar FN is still associated with the BCR.

Loss of FN fibrils reduces mesendoderm adhesion to the BCR and accelerates mesendodermal mantle closure

We also investigated the relationship between fibrillar FN and mesendoderm cells, which migrate along the BCR in association with FN fibrils. In normal gastrulae, mesendodermal cells comprise a circular mantle of tissue that migrates as a sheet over the assembled FN matrix of the BCR until the continuous leading edge of the mantle is drawn to a single point in the animal pole and fuses (Davidson et al., 2002; Winklbauer, 1990). This tissue is the precursor to structures such as head mesoderm, heart and blood. Cross-sections of the mesendodermal mantle revealed gaps at the boundary between the mesendoderm and the BCR in the absence of fibrils (Fig. 7B–C). After completion of mantle closure the tissue frequently detached from the BCR (Fig. 7D). However, as axial elongation proceeded, the mesendoderm was maintained as an intact tissue that populated the head and anterior-ventral regions of the embryo, giving rise to normal tissue derivatives. We were unable to image directly the migration velocity of the annular mesendodermal mantle in live 70 kD FN embryos due to the abnormally thick BCR. Instead, early and late gastrulae were fixed at defined time points and the BCRs peeled back to reveal the underlying mesendoderm. The mesendodermal mantles in embryos lacking FN fibrils were consistently more advanced than the mantles in control embryos (Fig. 7E) suggesting that while migration *per se* does not require fibrillar FN, the kinetics of mesendodermal mantle closure were accelerated in the absence of FN fibrils.

Discussion

In this study, we explored the formation of the nascent FN matrix and its normal transition to a 3D network of fibrils during gastrulation, and asked whether progressive changes in the physical properties of FN could regulate morphogenesis. We show that for some but not all cell movements, FN fibrils are functionally distinct from non-fibrillar and/or soluble-dimeric

forms of FN. These data suggest a mechanism for regulation of morphogenesis that has not been described previously *in vivo*.

The experimental approach used in the current report differs from the loss-of-function strategies employed in earlier *Xenopus* studies, which addressed the general functions of FN and/or integrins at gastrulation. The primary difference is that 70 kD FN expression alters neither FN expression nor the binding of secreted FN dimers to integrins at the cell surface. In contrast, previous studies used methods that either interfered with FN expression (e.g., morpholino knockdowns) or the binding of FN to integrins (e.g., blocking antibodies, dominant-negative integrin expression). In either instance, by preventing integrin engagement of FN normal adhesive and/or signal transduction events were disrupted. Correspondingly, 70 kD FN expression allowed us to ask what, if any phenotypic differences can be attributed specifically to the fibrillar state of FN matrix vs. simple engagement of FN dimers and integrins. Thus, the current data need to be considered in light of the previous results.

Gastrulation phenotypes resulting from morpholino knockdown of FN (Davidson et al., 2006) or direct inhibition of integrin-FN binding with mAbs (Marsden and DeSimone, 2001: 2003) are remarkably similar. The embryos exhibit delayed blastopore closure, fail to undergo normal axial extension and while the mesendoderm displays defects in BCR adhesion and migration the tissue is able to progress inward. Both radial cell intercalation in the BCR (Marsden and DeSimone, 2001) and mediolateral cell intercalation of axial and paraxial mesoderm (Marsden and DeSimone, 2003; Davidson et al., 2006) are inhibited when FN binding to integrins is blocked. Moreover, cells normally involved in radial and mediolateral intercalation movements lose polarized cell behaviors; spindle polarity and cleavage planes are disrupted in BCR cells and the normally bipolar protrusive dorsal mesoderm become multipolar protrusive (Marsden and DeSimone, 2003; Davidson et al., 2006). Despite defects in multiple gastrulation movements, blastopore closure eventually completes. The most likely current explanation is that convergent “thickening” driven by multipolar protrusive activity is sufficient to close the blastopore (Davidson et al., 2006; Keller and Shook, 2008).

The common thread among these studies is that FN is critical for the regulation and maintenance of at least three gastrulation movements: convergent extension, epiboly and mesendoderm migration. However, it was unclear whether the assembly state of the 3D FN matrix plays a role in regulating the underlying morphogenetic cell behaviors associated with these movements. For example, if simply disrupting integrin-FN engagement leads to dramatic changes in the protrusive activities of mediolaterally intercalating cells (Davidson et al., 2006), how might cell behaviors differ in response to fibrillar vs. non-fibrillar or soluble ligand, all three states of which make their appearance as matrix assembly proceeds during gastrulation?

There is mounting evidence that the 3D architecture of assembled ECMs can affect profoundly cell behavior, gene regulation, and even cellular pathologies (Darribère and Schwarzbauer, 2000; Engler et al., 2006; Green and Yamada, 2007; Nelson and Bissell, 2006; Pelham and Wang, 1997). Most studies of cell-ECM interactions have relied on cell culture systems utilizing planar adhesive ECM-substrates, or targeted ECM molecule loss-of-function analyses *in vivo*. However, many morphogenetic behaviors initiate during embryogenesis when the ECM is first being assembled and remodeled by the very tissues that require these ECM signals. FN function in development provides a good example of this coordinate “assembly and response” to the ECM. FN dimers bind to cell surfaces and assemble subsequently into fibrillar structures as morphogenesis proceeds. Although much is now known regarding the molecular and cellular steps in the process of assembly, the functional importance of these transitional states of matrix architecture to normal development and physiology has not been addressed.

FN fibril assembly states and in vivo consequences of failed assembly

How might transitional steps in the process of FN fibril assembly affect cell behaviors? There are several possibilities. First, macromolecular fibrillar networks of FN may transduce mechanical signals that are distinct from single FN dimers bound to cell surfaces. Second, the 3D organization of FN into fibrils may limit or promote access to binding sites on FN for transmembrane receptors such as integrins and syndecans, or for regions of FN that are involved in ECM protein-protein interactions. FN is known to undergo stretch-sensitive changes in conformation that have been proposed to regulate ECM assembly (Baneyx et al., 2002; Baneyx and Vogel, 1999; Erickson, 1994; Zhang et al., 1997) and cell adhesion (Katz et al., 2000). Third, the assembly of FN into fibrillar structures may change the local effective concentration of cell-binding sites within FN and, thus, binding avidity of integrins/syndecans. In the course of these studies, we were surprised to discover that early embryonic fibrillar FN has distinct biochemical properties from that of FN fibrils isolated at later stages (Fig. 2) or from tissue culture cells (McKeown-Longo and Mosher, 1983). Gastrula-stage fibrillar FN is soluble in deoxycholate (DOC) while fibrils assembled at later stages and by tissue culture cells are DOC insoluble. These data suggest that the early provisional FN matrix first assembled *in vivo*, may indeed have unique biochemical and mechanical properties, which in turn affect not only how cells and tissues respond to the matrix but also the kinetics of matrix remodeling at these stages (Davidson et al., 2008).

The relative amount of FN in contact with cells is another important factor to consider when addressing the functional consequences of the dynamic physical assembly state of FN *in vivo*. Because there is no apparent decrease in endogenous FN translation or FN dimer secretion into the blastocoel in the presence of 70 kD (Fig. 2G), it is unlikely that the integrins on the cells that normally assemble the FN matrix (i.e., BCR cells) are engaging less FN. However, it is reasonable to conclude that over time, FN binding to the BCR in the presence of 70 kD FN is saturable and limited by the number of integrins available at the BCR cell surface. This would explain why FN levels are equivalent in control and 70 kD FN embryos during early but not later stages of gastrulation (Fig. 3). In contrast, while FN-dimer binding to integrins at BCR cell surfaces is also saturable, FN-FN N-terminal interactions are able to proceed normally leading to the assembly of FN fibrils and further accumulation of FN. This assembly and accumulation of fibrils effectively increases the number of CCBD sites available to responding cells such as the mesendoderm as discussed below.

Some but not all gastrulation movements are sensitive to fibrillar state of FN

In the BCR, radial intercalation of multiple deep cell layers thins the roof tissue into a stratified layer of 2 cells in thickness by the end of gastrulation (Keller, 1980; Marsden and DeSimone, 2001). We demonstrated previously using function-blocking mAbs that inhibition of FN-integrin binding resulted in a failure of radial intercalation and BCR thinning (Marsden and DeSimone, 2001). In the current study we show that 70 kD FN inhibited the formation of FN fibrils and was sufficient to cause BCR thickening even though FN was still bound to integrins at the cell surface. As in the earlier antibody blocking experiments, 70 kD FN expression also resulted in misaligned mitotic spindles. Polarized cell division is required for a variety of morphogenetic movements such as avian primitive streak elongation (Wei and Mikawa, 2000), axial extension in the dorsal epiblast of zebrafish (Gong et al., 2004) and epiboly in *Xenopus* (Marsden and DeSimone, 2001). In normal BCRs, spindles are oriented parallel to the horizontal plane of the BCR and the resultant daughter cells remain within the plane of the tissue and do not contribute to thickening. In contrast, in the absence of FN, many cell divisions occur perpendicular to the plane of the BCR and this contributes to BCR thickness instead of thinning and horizontal spreading (i.e., epiboly). In the absence of FN fibrils, as in the FN loss of function analyses, spindle orientation was randomized and epiboly impaired. Thus, FN

assembly into a 3D fibrillar network is required for oriented cell division to proceed normally and promote BCR thinning and epiboly.

Mechanical signals can be transduced through the ECM at both molecular (i.e., through individual protein complexes or pathways) and macro- (i.e., across a group of cells or tissues) scales (Ingber, 2006). One function of the macro-scale fibrillar network of FN assembled along the BCR may be the maintenance of tissue tension. Mechanical coupling of the ECM to the cytoskeleton via integrins could help orient mitotic spindles parallel to the plane of assembled fibrils. Mechanical regulation of oriented cell division has been shown previously to occur in human capillary endothelial cells (Maniotis et al., 1997). Moreover, maintenance of tension in the BCR through a fibrillar FN network may stabilize cell-cell interactions required for radial intercalation of deep layer cells and epibolic spreading of the tissue. In the presence of 70 kD FN, BCR cells became rounded instead of polygonal and the BCR thickened instead of thinning and spreading (Fig. 8A). The rounded appearance of BCR cells suggests that cell-cell contact and tissue tension were reduced in the absence of fibrils. In previous studies, we demonstrated that integrin-FN engagement regulates cadherin-mediated behaviors such as cell sorting and cell intercalation (Marsden and DeSimone, 2001; Marsden and DeSimone, 2003). Based on the current findings, we now appreciate that integrin-FN engagement is alone insufficient, and that the physical state of the macromolecular network of fibrillar FN is needed to promote BCR thinning and epiboly.

It is important to note that FN fibrils are asymmetrically localized in the late blastula and early gastrula with fibrillogenesis occurring only on the BCR and not the blastocoel floor. Consequently, if the fibrillar network is involved in maintaining tissue tension as we propose, then the absence of FN fibrils would likely result in a more uniform distribution of tissue tension along the entire blastocoel wall. One prediction of a more symmetrical distribution of tissue tension would be a change in the shape of the blastocoel from hemispheric to spherical. Indeed, we observed that the normally “flat” floor of the blastocoel bulged toward the vegetal pole when fibrillogenesis was inhibited and the blastocoel become more spherical (Fig. 6G, Fig. 8A). Thus, we hypothesize that a lack of fibrils results in a more symmetric distribution of tissue tension in the blastocoel overall while reduced tissue tension in the BCR results in rounded cell shapes, misaligned spindles and failure of radial cell intercalation leading to BCR thickening. In short, we propose that FN fibrils across the surface of the BCR normally serve a mechanical function to maintain tissue-level tension that is important for BCR thinning. A significant future challenge will be to measure directly changes in tissue tension and stiffness in the presence or absence of fibrillar FNs.

One alternative explanation is that loss of FN fibrils removes a matrix-bound signaling molecule or disrupts a signal gradient that normally directs the orientation of cell division planes. Mis-oriented spindles would then lead to thickening of the BCR. We are currently unable to distinguish whether spindle mis-orientation is a cause of BCR thickening or a consequence of reduced tissue tension in the BCR. The relationship between maintenance of tension/substrate rigidity and planar cell division is an interesting problem that will require further investigation.

In contrast to the observed defect in epiboly, convergent extension appeared unaffected in whole embryos that lacked FN fibrils. In addition, devitellinized 70 kD FN embryos exogastrulated and elongated, further suggesting that convergent extension was normal or possibly even enhanced in the absence of fibrils. These phenotypes were surprising because as discussed, morpholino knockdowns of FN block mediolateral cell intercalation movements that drive convergent extension (Davidson et al., 2006). We have proposed previously that FN functions by biasing the number and frequency of cellular protrusions along the mediolateral axis (Davidson et al., 2006). In the absence of FN, bipolar protrusive activity is disrupted and

the tissue converges and thickens instead of converging and extending along the A-P axis. Bipolar protrusive activity in explants obtained from embryos injected with FN morpholino were rescued by placing the explants on a non-fibrillar FN substrate (Davidson et al., 2006). This supports the conclusion that FN binding to integrins at cell surfaces is required for convergent extension but that fibrillar FN is not. Nonetheless, in the presence of 70 kD FN, non-fibrillar FN continues to accumulate and define tissue boundaries (e.g., notochord- somite; Fig 5F,H,I,K) and thus, may have a role in other tissue-level morphogenetic processes.

The ability of 70 kD FN embryos to undergo convergent extension may explain why blastopore closure eventually completes in most cases, and why embryos expressing 70 kD FN in the DMZ alone are able to close their blastopores on time relative to controls. In fact, in 70 kD FN embryos, the blastopore remains open as if stalled and then closes rapidly 2–3 hours later as if purse strings were being drawn (Fig. 4B and data not shown). This release from stalling coincides with the progression of convergent extension movements in the DMZ, which has been proposed as the primary driving force behind blastopore closure (Ewald et al., 2004;Keller and Danilchik, 1988) in addition to other contributing factors such as convergent thickening (Keller and Danilchik, 1988), mesoderm involution (Keller and Jansa, 1992) and vegetal rotation (Winklbauer and Schürfeld, 1999).

FN fibrils regulate mesendodermal mantle closure

The involvement of FN in amphibian mesendoderm cell migration has been the subject of several classic and more recent studies (Boucaut and Darribère, 1983; Boucaut et al., 1985; Darribère and Schwarzbauer, 2000; Davidson et al., 2002; Nagel and Winklbauer, 1999). Here we reinvestigated this question by asking specifically what role FN fibrils may play in promoting mesendoderm migration. Loss of FN function in *Xenopus* results in severe defects in mesendodermal derivatives that include heart, gut and blood (Davidson et al., 2006; Marsden and DeSimone, 2001), thus, we were surprised to observe no obvious defects in mesendodermal derivatives in embryos lacking FN fibrils following 70 kD FN expression. In fact, mesendodermal mantle closure was accelerated in *Xenopus* embryos lacking FN fibrils (Fig. 7). A previous study using urodele embryos reported that a non-fibrillar chimeric matrix composed of endogenous FN and recombinant rat FN fusion proteins inhibited mesoderm migration by perturbing cell spreading (Darribère and Schwarzbauer, 2000). In contrast, our findings demonstrate that migration *per se* proceeds in the absence of fibrillar FN but that the kinetics of cell migration depends on the physical assembly state of the matrix. These disparate results may reflect significant differences in urodele and anuran gastrulation movements (e.g., single cell vs. cell sheet migration) and/or the different experimental approaches used in these studies.

Cell migration speed on defined non-fibrillar ECM substrates *in vitro* is dependent on ECM molecule concentration (Palecek et al., 1997). Both low and high extremes of ECM substrate concentration can inhibit cell migration by regulating adhesive strength (Palecek et al., 1997). Migration is observed at intermediate adhesion levels, which favor a “balance” of cell attachment and detachment to promote cell locomotion. In our system, the minimum density of FN coating needed for mesendodermal cells to attach to artificial substrate supports maximal cell migration speed and as expected, increasing the FN density causes migration speed to decrease (Fig. 8B). Simply put, too much FN decreases migration speed *in vitro* and one interpretation of our results is that a similar principle is involved in regulating migration speed in the embryo.

Our data suggest that FN fibrils on the BCR normally slow mesendoderm migration. In fact, in normal embryos, FN fibrils are more densely packed on the “free” surface of the BCR in early-mid gastrulae compared to regions of the BCR that are overlapped with migrating mesendoderm (Davidson et al., 2004). We have shown that as the fibrillar matrix matures and

becomes more densely packed with time, more CCBD sites are predicted to be available (i.e., per unit area of the BCR) in control embryos relative to those expressing 70 kD FN (Fig. 3). Dense FN fibrils may favor cell attachment at the expense of cell detachment needed for locomotion. Our results indicate that mesendoderm adhesion to BCRs is reduced but not inhibited in embryos lacking fibrils (Fig. 7C–D). The accelerated mesendoderm mantle closure observed under these conditions suggests that the fibrillar architecture of the matrix normally slows the rate of mesendoderm migration in control embryos. Thus, we propose that the rate of mesendoderm mantle closure along the BCR is dependent on FN fibril density, which is likely altered by the mesendoderm (Davidson et al., 2004; 2008) resulting in observed migration optima in this system. BCR thickening in 70 kD FN embryos also contributes to the rate of mantle closure because the blastocoel radius is shortened slightly thus reducing the distance from equator to animal pole, but this alone is insufficient to account for the degree of accelerated mantle closure reported.

Mechanisms of fibril-dependent and independent cell behaviors

We propose that FN fibrils play a mechanical-adhesive role that promotes or in some contexts, restricts directed cell movements. Such functions complement the ability of non-fibrillar or soluble forms of FN to stimulate or repress morphogenetic cell movements. This may occur through changes in the engagement of transmembrane matrix receptors with subsequent affects on cell signaling and cytoskeletal organization. Initial binding of dimeric FN to cell surfaces (i.e., via integrins) is not affected by 70 kD FN. However, less total FN relative to controls accumulates at the surfaces of these cells over time because FN-FN assembly and fibril formation are inhibited. As a result, it is possible that the full complement of integrins, syndecans and/or other proteins normally engaged by a fibrillar matrix is altered in the presence of 70kD FN. Alternatively, the numbers of receptors bound under normal fibrillar and non-fibrillar (i.e., 70 kD FN) conditions may be comparable but differences in binding avidity (e.g., distribution and clustering of receptors) and/or affinity for FN may reflect differences in assembly state. Distinguishing the contributions of the mechanical properties of a fibrillar matrix from these likely differences in transmembrane receptor engagement represent a major challenge that will require both cell culture and whole embryo/tissue level analyses.

The regulated arrangement of FN into fibrillar networks may serve to direct and/or support multiple functions during development. A fibrillar network could act as a mechano-sensitive “switch” that transduces and maintains mechanical signals between the cells and the extracellular microenvironment. For example, cytoskeletal contractility could increase force on integrins bound to FNs leading to tension-induced conformational changes in the protein. This could, in turn, expose cryptic binding sites for additional cell surface receptors, other matrix proteins or soluble factors (Vogel, 2006). Cytoskeletal contractility may also influence the local stiffness of the FN matrix. Alternatively, the fibrillar matrix may relay physical forces such as blastocoel hydrostatic pressure, which may help maintain tissue tension across the BCR. Mechanical regulation is not the only potential function of fibrillar FN. Fibrillogenesis may also serve to regulate the availability of specific binding sites by either concealing biologically active sites or by increasing the density of binding sites available for receptors such as integrins. These binding sites in FN could influence the behaviors of both the cells that assemble the FN matrix (e.g., BCR) and the cells that respond to the matrix (e.g., the migratory mesendoderm).

Another interesting possibility is that FN binding to integrins and syndecans can influence non-canonical Wnt signaling (Marsden and DeSimone, 2001; Muñoz et al., 2006) and cadherin adhesion (Dzamba et al., submitted). While FN appears to be necessary for mediolateral intercalation it alone is not sufficient to drive this behavior in the absence of Wnt/PCP signaling (Davidson et al., 2006), which has been shown to be required for convergent extension in

Xenopus (Smith et al., 2000; Wallingford and Harland, 2001) and other systems (Keller, 2002; Torban et al., 2004). Recent data demonstrates a direct connection between Wnt/PCP signaling and the assembly of FN matrices at gastrulation, which in part may explain the dual requirement of Wnt/PCP and FN, at least in terms of convergence and extension movements (Dzamba et al., submitted; Goto et al., 2005). Whether the physical state of the FN matrix might influence cross-talk between these pathways is unclear. Because cell surface-bound FN dimers are less effective than FN fibrils in clustering integrins (Wierzbicka-Patynowski and Schwarzbauer, 2003), the activation of some outside-in signaling events may be attenuated in the absence of FN fibrils. Nevertheless, convergent extension progresses in the absence of a fibrillar matrix suggesting that extensive integrin clustering is not a prerequisite step for normal mediolateral intercalation behaviors.

We have demonstrated that the 3D organization of assembled FN matrices has important consequences for regulating normal morphogenetic movements in embryos. FN fibrils are required for epiboly but not convergent extension. Moreover, FN fibrillogenesis and remodeling may regulate the migratory behavior of the mesendoderm. These studies provide *in vivo* evidence for differences in physical properties of extracellular microenvironments that instruct distinct morphogenetic cell behaviors.

Supplementary Material

Refer to Web version on PubMed Central for supplementary material.

Acknowledgments

We thank Maureen Bjerke and Karoly Jakab for comments on the manuscript and Fred Simon for excellent frog care. We also thank Rick Horwitz, Judith White, Ray Keller, Barry Gumbiner and Martin Schwartz for helpful advice and discussion. This work was supported by USPHS grant HD26402.

References

Baneyx G, Baugh L, Vogel V. Fibronectin extension and unfolding within cell matrix fibrils controlled by cytoskeletal tension. Proc Natl Acad Sci USA 2002;99:5139–43. [PubMed: 11959962]

Baneyx G, Vogel V. Self-assembly of fibronectin into fibrillar networks underneath dipalmitoyl phosphatidylcholine monolayers: role of lipid matrix and tensile forces. Proc Natl Acad Sci USA 1999;96:12518–23. [PubMed: 10535954]

Barcellos-Hoff MH, Aggeler J, Ram TG, Bissell MJ. Functional differentiation and alveolar morphogenesis of primary mammary cultures on reconstituted basement membrane. Development 1989;105:223–35. [PubMed: 2806122]

Boucaut JC, Darribère T. Fibronectin in early amphibian embryos. Migrating mesodermal cells contact fibronectin established prior to gastrulation. Cell Tissue Res 1983;234:135–45. [PubMed: 6640612]

Boucaut JC, Darribère T, Li SD, Boulekbache H, Yamada KM, Thiery JP. Evidence for the role of fibronectin in amphibian gastrulation. Journal of embryology and experimental morphology. 1985;89 (Suppl):211–27.

Darribère T, Schwarzbauer JE. Fibronectin matrix composition and organization can regulate cell migration during amphibian development. Mech Dev 2000;92:239–50. [PubMed: 10727862]

Davidson LA, Dzamba BD, Keller R, DeSimone DW. Live imaging of cell protrusive activity, and extracellular matrix assembly and remodeling during morphogenesis in the frog, *Xenopus laevis.* Dev Dyn 2008;15:15.

Davidson LA, Hoffstrom BG, Keller R, DeSimone DW. Mesendoderm extension and mantle closure in *Xenopus laevis* gastrulation: combined roles for integrin α5β1, fibronectin, and tissue geometry. Dev Biol 2002;242:109–29. [PubMed: 11820810]

Davidson LA, Keller R, DeSimone DW. Assembly and remodeling of the fibrillar fibronectin extracellular matrix during gastrulation and neurulation in *Xenopus laevis*. Dev Dyn 2004;231:888–95. [PubMed: 15517579]

Davidson LA, Marsden M, Keller R, DeSimone DW. Integrin alpha5beta1 and fibronectin regulate polarized cell protrusions required for *Xenopus* convergence and extension. Curr Biol 2006;16:833–44. [PubMed: 16682346]

DeSimone DW, Norton PA, Hynes RO. Identification and characterization of alternatively spliced fibronectin mRNAs expressed in early *Xenopus* embryos. Dev Biol 1992;149:357–69. [PubMed: 1730390]

Dzamba BJ, Jakab KR, Marsden M, Schwartz MA, DeSimone DW. Cadherin adhesion, tissue tension and non-canonical Wnt signaling regulate fibronectin matrix organization. submitted.

Engler AJ, Sen S, Sweeney HL, Discher DE. Matrix elasticity directs stem cell lineage specification. Cell 2006;126:677–89. [PubMed: 16923388]

Erickson HP. Reversible unfolding of fibronectin type III and immunoglobulin domains provides the structural basis for stretch and elasticity of titin and fibronectin. Proc Natl Acad Sci USA 1994;91:10114–8. [PubMed: 7937847]

Ewald AJ, Peyrot SM, Tyszka JM, Fraser SE, Wallingford JB. Regional requirements for Dishevelled signaling during *Xenopus* gastrulation: separable effects on blastopore closure, mesendoderm internalization and archenteron formation. Development 2004;131:6195–209. [PubMed: 15548584]

Fogerty FJ, Akiyama SK, Yamada KM, Mosher DF. Inhibition of binding of fibronectin to matrix assembly sites by anti-integrin (alpha 5 beta 1) antibodies. J Cell Biol 1990;111:699–708. [PubMed: 2380248]

George EL, Georges-Labouesse EN, Patel-King RS, Rayburn H, Hynes RO. Defects in mesoderm, neural tube and vascular development in mouse embryos lacking fibronectin. Development 1993;119:1079–91. [PubMed: 8306876]

Georges-Labouesse EN, George EL, Rayburn H, Hynes RO. Mesodermal development in mouse embryos mutant for fibronectin. Dev Dyn 1996;207:145–56. [PubMed: 8906418]

Gong Y, Mo C, Fraser SE. Planar cell polarity signaling controls cell division orientation during zebrafish gastrulation. Nature 2004;430:689–93. [PubMed: 15254551]

Goto T, Davidson L, Asashima M, Keller R. Planar cell polarity genes regulate polarized extracellular matrix deposition during frog gastrulation. Curr Biol 2005;15:787–93. [PubMed: 15854914]

Green JA, Yamada KM. Three-dimensional microenvironments modulate fibroblast signaling responses. Adv Drug Deliv Rev 2007;59:1293–8. [PubMed: 17825946]

Harland RM. *In situ* hybridization: an improved whole-mount method for Xenopus embryos. Methods Cell Biol 1991;36:685–95. [PubMed: 1811161]

Ingber DE. Cellular mechanotransduction: putting all the pieces together again. FASEB J 2006;20:811–27. [PubMed: 16675838]

Katz BZ, Zamir E, Bershadsky A, Kam Z, Yamada KM, Geiger B. Physical state of the extracellular matrix regulates the structure and molecular composition of cell-matrix adhesions. Mol Biol Cell 2000;11:1047–60. [PubMed: 10712519]

Keller R. Shaping the vertebrate body plan by polarized embryonic cell movements. Science 2002;298:1950–4. [PubMed: 12471247]

Keller R. Mechanisms of elongation in embryogenesis. Development 2006;133:2291–302. [PubMed: 16720874]

Keller R, Danilchik M. Regional expression, pattern and timing of convergence and extension during gastrulation of *Xenopus laevis*. Development 1988;103:193–209. [PubMed: 3197629]

Keller R, Davidson L, Edlund A, Elul T, Ezin M, Shook D, Skoglund P. Mechanisms of convergence and extension by cell intercalation. Philos Trans R Soc Lond B Biol Sci 2000;355:897–922. [PubMed: 11128984]

Keller R, Jansa S. *Xenopus* Gastrulation without a blastocoel roof. Dev Dyn 1992;195:162–76. [PubMed: 1301081]

Keller R, Shook D. Dynamic determinations: patterning the cell behaviours that close the amphibian blastopore. Philos Trans R Soc Lond B Biol Sci 2008;363:1317–32. [PubMed: 18192174]

Keller RE. Time-lapse cinemicrographic analysis of superficial cell behaviour during and prior to gastrulation in *Xenopus laevis*. J Morph 1978;157:223–247.

Keller RE. The cellular basis of epiboly: an SEM study of deep-cell rearrangement during gastrulation in *Xenopus laevis*. Journal of embryology and experimental morphology 1980;60:201–34. [PubMed: 7310269]

Lee EY, Lee WH, Kaetzel CS, Parry G, Bissell MJ. Interaction of mouse mammary epithelial cells with collagen substrata: regulation of casein gene expression and secretion. Proc Natl Acad Sci USA 1985;82:1419–23. [PubMed: 3856271]

Lee G, Hynes R, Kirschner M. Temporal and spatial regulation of fibronectin in early *Xenopus* development. Cell 1984;36:729–40. [PubMed: 6697394]

Maniotis AJ, Bojanowski K, Ingber DE. Mechanical continuity and reversible chromosome disassembly within intact genomes removed from living cells. J Cell Biochem 1997;65:114–30. [PubMed: 9138086]

Marsden M, DeSimone DW. Regulation of cell polarity, radial intercalation and epiboly in *Xenopus*: novel roles for integrin and fibronectin. Development 2001;128:3635–47. [PubMed: 11566866]

Marsden M, DeSimone DW. Integrin-ECM interactions regulate cadherin-dependent cell adhesion and are required for convergent extension in *Xenopus*. Curr Biol 2003;13:1182–91. [PubMed: 12867028]

Mayor R, Morgan R, Sargent MG. Induction of the prospective neural crest of *Xenopus*. Development 1995;121:767–77. [PubMed: 7720581]

McBeath R, Pirone DM, Nelson CM, Bhadriraju K, Chen CS. Cell shape, cytoskeletal tension, and RhoA regulate stem cell lineage commitment. Dev Cell 2004;6:483–95. [PubMed: 15068789]

McDonald JA, Quade BJ, Broekelmann TJ, LaChance R, et al. Fibronectin's cell-adhesive domain and an amino-terminal matrix assembly domain participate in its assembly into fibroblast pericellular matrix. J Biol Chem 1987;262:2957–2967. [PubMed: 3818629]

McKeown-Longo PJ, Mosher DF. Binding of plasma fibronectin to cell layers of human skin fibroblasts. J Cell Biol 1983;97:466–72. [PubMed: 6309861]

McKeown-Longo PJ, Mosher DF. Interaction of the 70,000-mol-wt amino-terminal fragment of fibronectin with the matrix-assembly receptor of fibroblasts. J Cell Biol 1985;100:364–74. [PubMed: 3155749]

Mosher DF, Sottile J, Wu C, McDonald JA. Assembly of extracellular matrix. Curr Opin Cell Biol 1992;4:810–8. [PubMed: 1419058]

Muñoz R, Moreno M, Oliva C, Orbenes C, Larraín J. Syndecan-4 regulates non-canonical Wnt signaling and is essential for convergent and extension movements in *Xenopus* embryos. Nat Cell Biol 2006;8:492–500. [PubMed: 16604063]

Nagel M, Winklbauer R. Establishment of substratum polarity in the blastocoel roof of the *Xenopus* embryo. Development 1999;126:1975–84. [PubMed: 10101131]

Nelson CM, Bissell MJ. Of extracellular matrix, scaffolds, and signaling: tissue architecture regulates development, homeostasis, and cancer. Annu Rev Cell Dev Biol 2006;22:287–309. [PubMed: 16824016]

Nieuwkoop, PD.; Faber, J. Normal Table of *Xenopus laevis* (Daudin). Garland Publishing Inc; New York: 1994.

Palecek SP, Loftus JC, Ginsberg MH, Lauffenburger DA, Horwitz AF. Integrin-ligand binding properties govern cell migration speed through cell-substratum adhesiveness. Nature 1997;385:537–40. [PubMed: 9020360]

Pelham RJ, Wang Y. Cell locomotion and focal adhesions are regulated by substrate flexibility. Proc Natl Acad Sci USA 1997;94:13661–5. [PubMed: 9391082]

Ramos JW, DeSimone DW. *Xenopus* embryonic cell adhesion to fibronectin: position-specific activation of RGD/synergy site-dependent migratory behavior at gastrulation. J Cell Biol 1996;134:227–40. [PubMed: 8698817]

Schwarzbauer JE, Sechler JL. Fibronectin fibrillogenesis: a paradigm for extracellular matrix assembly. Curr Opin Cell Biol 1999;11:622–7. [PubMed: 10508649]

Shih J, Keller R. Cell motility driving mediolateral intercalation in explants of *Xenopus laevis*. Development 1992;116:901–14. [PubMed: 1295743]

Smith JC, Conlon FL, Saka Y, Tada M. Xwnt11 and the regulation of gastrulation in *Xenopus*. Philos Trans R Soc Lond B Biol Sci 2000;355:923–30. [PubMed: 11128985]

Torban E, Kor C, Gros P. Van Gogh-like2 (Strabismus) and its role in planar cell polarity and convergent extension in vertebrates. Trends Genet 2004;20:570–7. [PubMed: 15475117]

Trinh LA, Stainier DY. Fibronectin regulates epithelial organization during myocardial migration in zebrafish. Dev Cell 2004;6:371–82. [PubMed: 15030760]

Vogel V. Mechanotransduction involving multimodular proteins: converting force into biochemical signals. Annual review of biophysics and biomolecular structure 2006;35:459–88.

Wallingford JB, Harland RM. *Xenopus* Dishevelled signaling regulates both neural and mesodermal convergent extension: parallel forces elongating the body axis. Development 2001;128:2581–92. [PubMed: 11493574]

Wei Y, Mikawa T. Formation of the avian primitive streak from spatially restricted blastoderm: evidence for polarized cell division in the elongating streak. Development 2000;127:87–96. [PubMed: 10654603]

Wierzbicka-Patynowski I, Schwarzbauer JE. The ins and outs of fibronectin matrix assembly. J Cell Sci 2003;116:3269–76. [PubMed: 12857786]

Winklbauer R. Mesodermal cell migration during *Xenopus* gastrulation. Dev Biol 1990;142:155–68. [PubMed: 2227092]

Winklbauer R, Schürfeld M. Vegetal rotation, a new gastrulation movement involved in the internalization of the mesoderm and endoderm in *Xenopus*. Development 1999;126:3703–13. [PubMed: 10409515]

Yang JT, Bader BL, Kreidberg JA, Ullman-Culleré M, Trevithick JE, Hynes RO. Overlapping and independent functions of fibronectin receptor integrins in early mesodermal development. Dev Biol 1999;215:264–77. [PubMed: 10545236]

Zhang Q, Magnusson MK, Mosher DF. Lysophosphatidic acid and microtubule-destabilizing agents stimulate fibronectin matrix assembly through Rho-dependent actin stress fiber formation and cell contraction. Mol Biol Cell 1997;8:1415–25. [PubMed: 9285815]

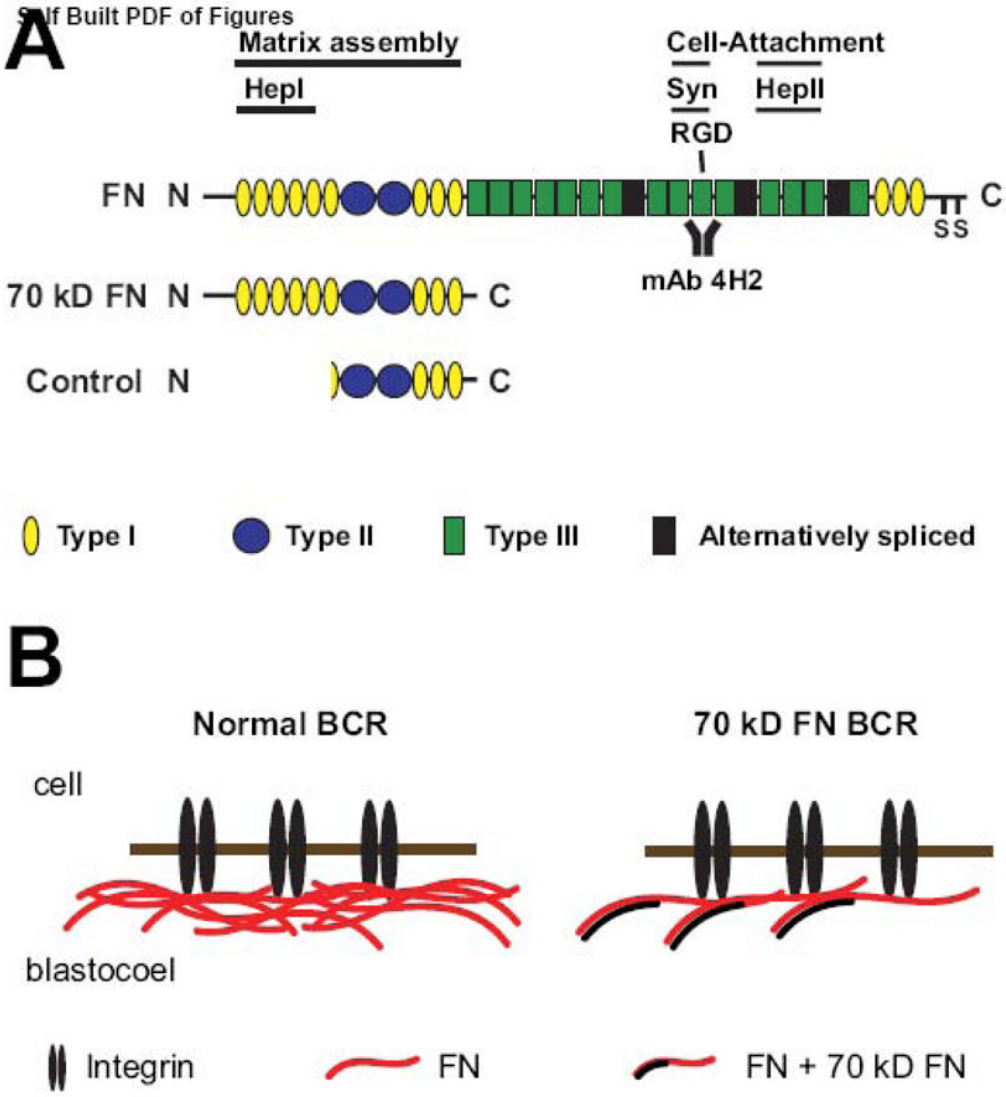

Fig. 1.

Fibronectin constructs and strategy for inhibition of FN fibril assembly. (A) Schematic of *Xenopus laevis* FN and the corresponding control and 70 kD FN constructs used in this study. Location of epitope for mAb 4H2 in Type III_{10} is indicated. (B) Representation of presumed mechanism of FN fibril inhibition by 70 kD FN based on the current literature. 70 kD FN binds to the N-terminal matrix assembly domain of endogenously expressed FN, thus blocking FN-FN interactions and fibrillogenesis but not the initial binding of endogenous dimeric FN to integrins at the cell surface. Additional FN dimers are accumulated into the BCR matrix as fibrillogenesis and gastrulation proceed in normal embryos but not in 70 kD FN embryos. This is possible even though the numbers of integrins engaged with FN under both conditions are equivalent.

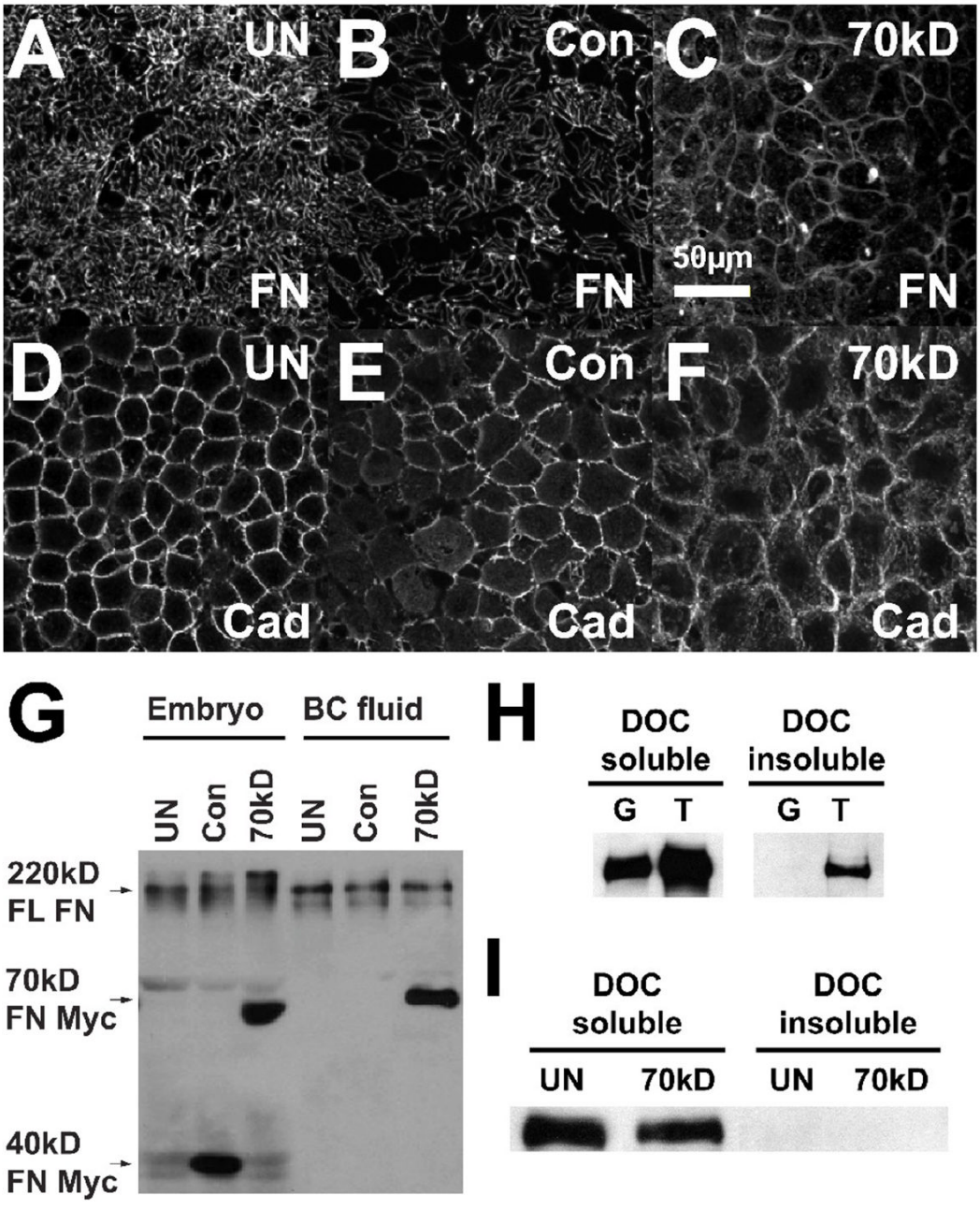

Fig. 2.

Expression of 70 kD FN blocks FN fibrillogenesis but does not perturb expression and secretion of endogenous FN. (A-F) Extended focus confocal micrographs (thickness ~2 μm) of *en face* BCRs immunostained for FN or C-Cadherin. (G) Western blot of total embryo lysates and extracted blastocoel fluid probed with pAb 32F-J directed against endogenous FN (FL FN), and the anti-Myc mAb 9E10 that recognizes both the 70 kD and 40 kD myc-tagged FN constructs (FN-Myc). (H) Western blot of DOC extracted embryos probed for FN. DOC insoluble FN can be detected at tailbud [T] but not gastrula [G] stages. (I) Western blot of DOC extracted control and 70 kD FN gastrula stage embryos confirmed that FN is DOC soluble under both conditions. (UN: uninjected; con: control construct injected embryos; 70 kD: 70 kD FN-Myc injected embryos)

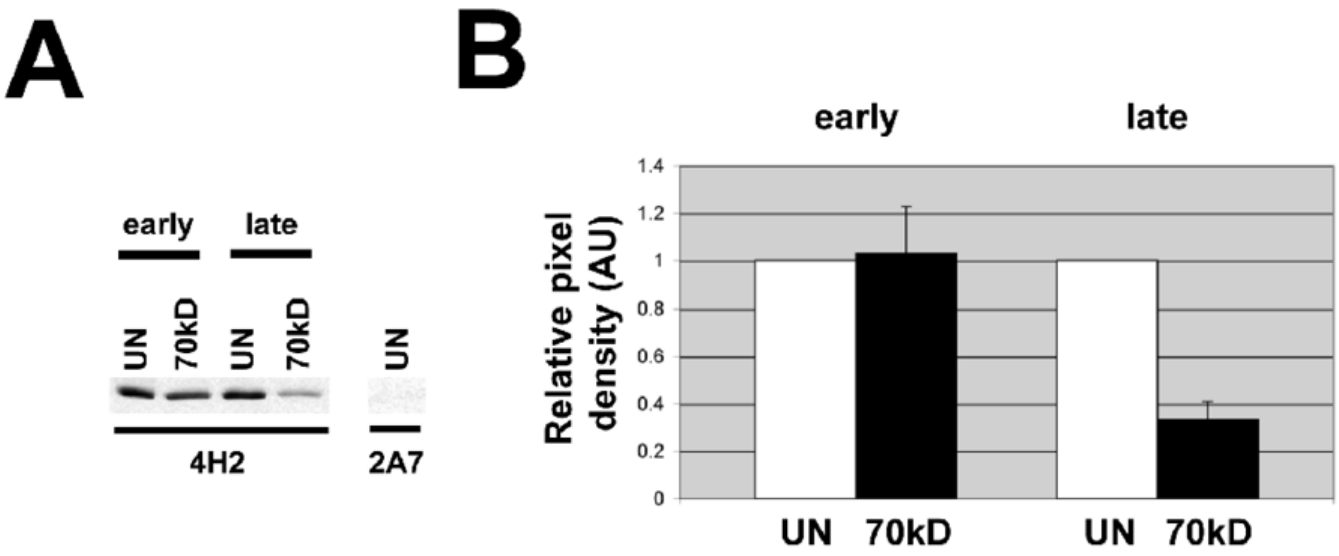

Fig. 3.

Levels of total endogenous FN associated with BCR cell surfaces in the presence or absence of 70 kD FN as development proceeds. (A) Live, isolated BCRs were incubated with an anti-FN mAb 4H2 that recognizes the central cell binding domain (CCBD) where FN binds integrin α5β1. BCRs were washed, extracted and run on a non-reduced Western blot and then probed for anti-mouse IgG in order to detect the 4H2 antibody. BCRs incubated with and antibody directed against a cytoplasmic protein (anti-FAK mAb 2A7) was used as a negative control. At early stages (stg. 10–10.5) when fibril assembly begins, 4H2 binding to uninjected (UN) and 70 kD FN (70 kD) caps is comparable indicating that dimeric FN binding to integrins at BCR cell surfaces is equivalent. By late gastrula stages (stg. 11.5), 4H2 binding to 70 kD FN caps was ~30% that of UN control caps. In the 70 kD FN embryos, additional accumulation of FN is blocked, presumably due to limited availability of unoccupied integrins at the cell surface and the failure to form FN multimers. (B) Quantification of 4H2 binding to BCRs. Values (relative pixel densities of scanned gels) were normalized to control levels of FN, (N=4). Error bars are ±SEM

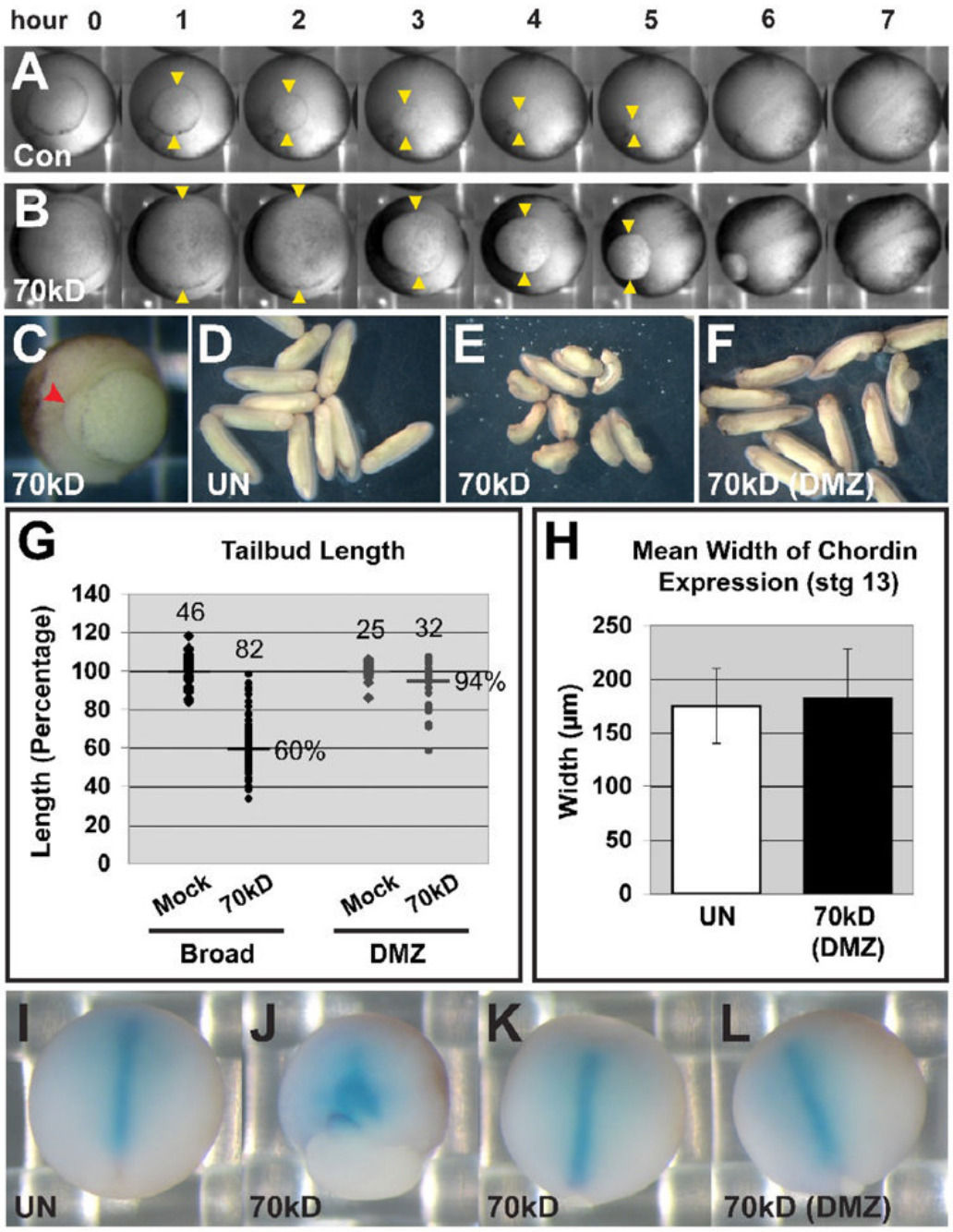

Fig. 4.

Blastopore closure and epiboly but not axial extension are defective in embryos expressing 70 kD FN. (A-B) Time-matched frames from movies of blastopore closure in representative sibling embryos expressing control (Con) or 70 kD FN (70 kD) constructs. Yellow arrowheads mark the approximate diameters of the blastopores. (C) A representative 70 kD FN gastrula with delayed blastopore closure initiates a putative second blastopore lip (red arrowhead). (D–F) Tailbud stage embryos; (D) uninjected (UN), (E) injected with 70 kD FN into both blastomeres at 2-cell stage, or (F) into the marginal region of two presumptive dorsal blastomeres at the 4-cell stage (DMZ: dorsal marginal zone). (G) Quantification of 70 kD FN tailbud embryo lengths normalized to the mean length of mock injected (dextran only) tailbud

embryos from each batch. The horizontal lines represent the mean tailbud lengths. Numbers of all tailbud embryos analyzed are listed above each group. (H) Quantification of the mean width of the axial marker Chordin from *in situ* hybridizations. Error bars are ±SD (n= 9–10). (I–L) *In situ* hybridizations after completion of gastrulation (stg. 13) showing localization of Chordin mRNAs. Axial elongation in embryos expressing (L) 70 kD FN in the DMZ are comparable to (I) uninjected embryos. Broad expression of 70 kD FN results in two phenotypes: (J) embryos that fail to complete blastopore closure show a wide pattern of Chordin expression, and (K) embryos that complete blastopore closure express Chordin in a similar pattern to uninjected controls.

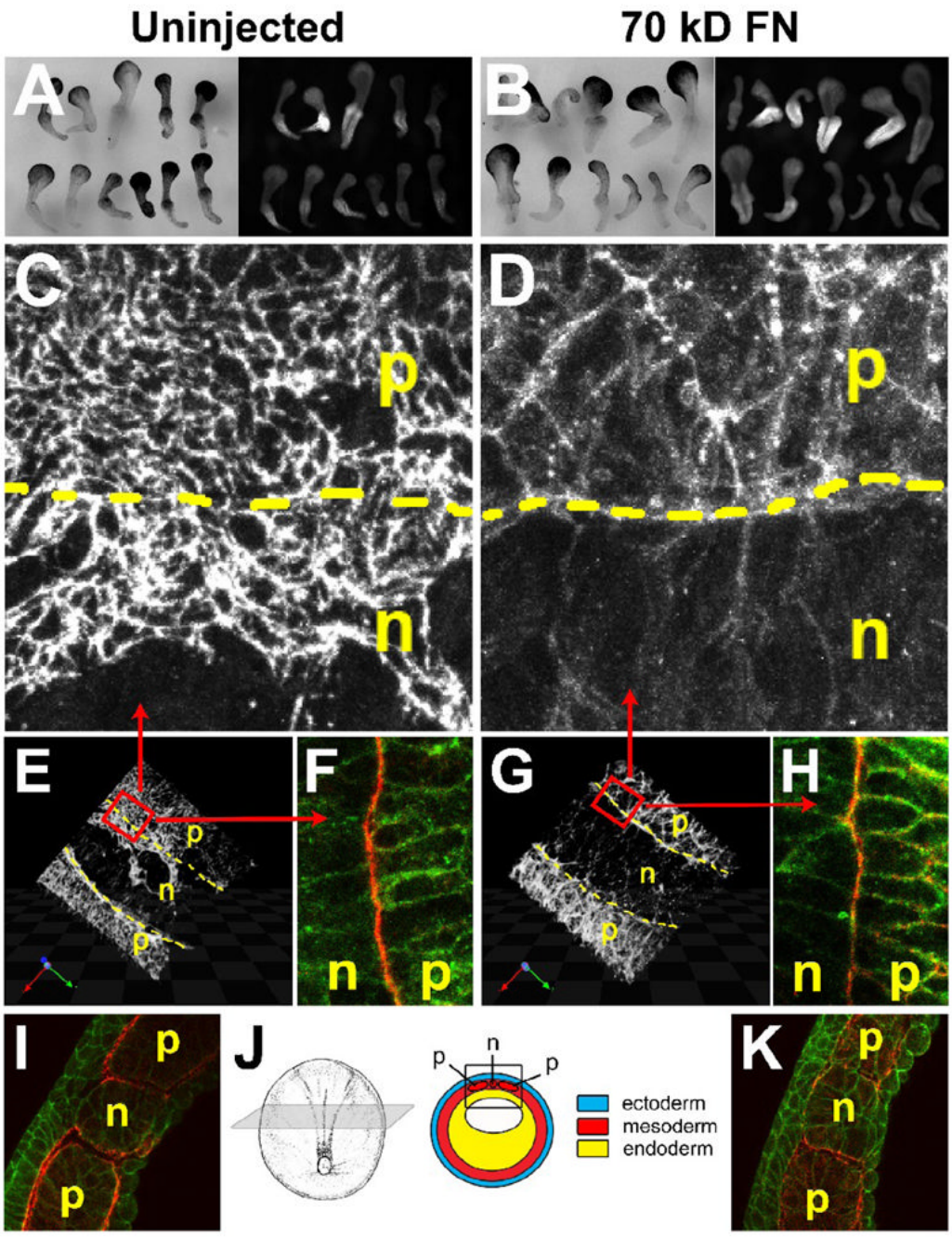

Fig. 5.

Fibrillar FN is not required for convergent extension in explants or whole embryos. (A–B) Keller sandwich explants made from control or 70 kD FN embryos from 6 experiments (*n*=2–5 per group) and immunostained for FN. Bright-field images at left and corresponding immunofluorescence at right. (C-D) High magnification, extended focus views of FN immunostaining from Keller explants, at the boundary (yellow dashes) of the notochord (n) and presomitic mesoderm (p). (E and G) 3-D rendered images of FN immunostaining from confocal z-series (~100 μm depth) obtained from the representative Keller sandwiches shown in (C) and (D). (F & H) Single confocal slice from within the through-focus region indicated by the red boxes in (E) and (G), immunostained for C-Cad (green) and FN (red). Movies of

the z-series-through-focus and 3D rendering are available online (supplemental Movies 1 and 2). (I–K) Cross section of late stg. 12 gastrulae through the neural plate region (J) of uninjected (I) and 70 kD FN (K) embryos immunostained for C-Cad (green) and FN (red). Diagram at left in (J) after (Nieuwkoop and Faber, 1994).

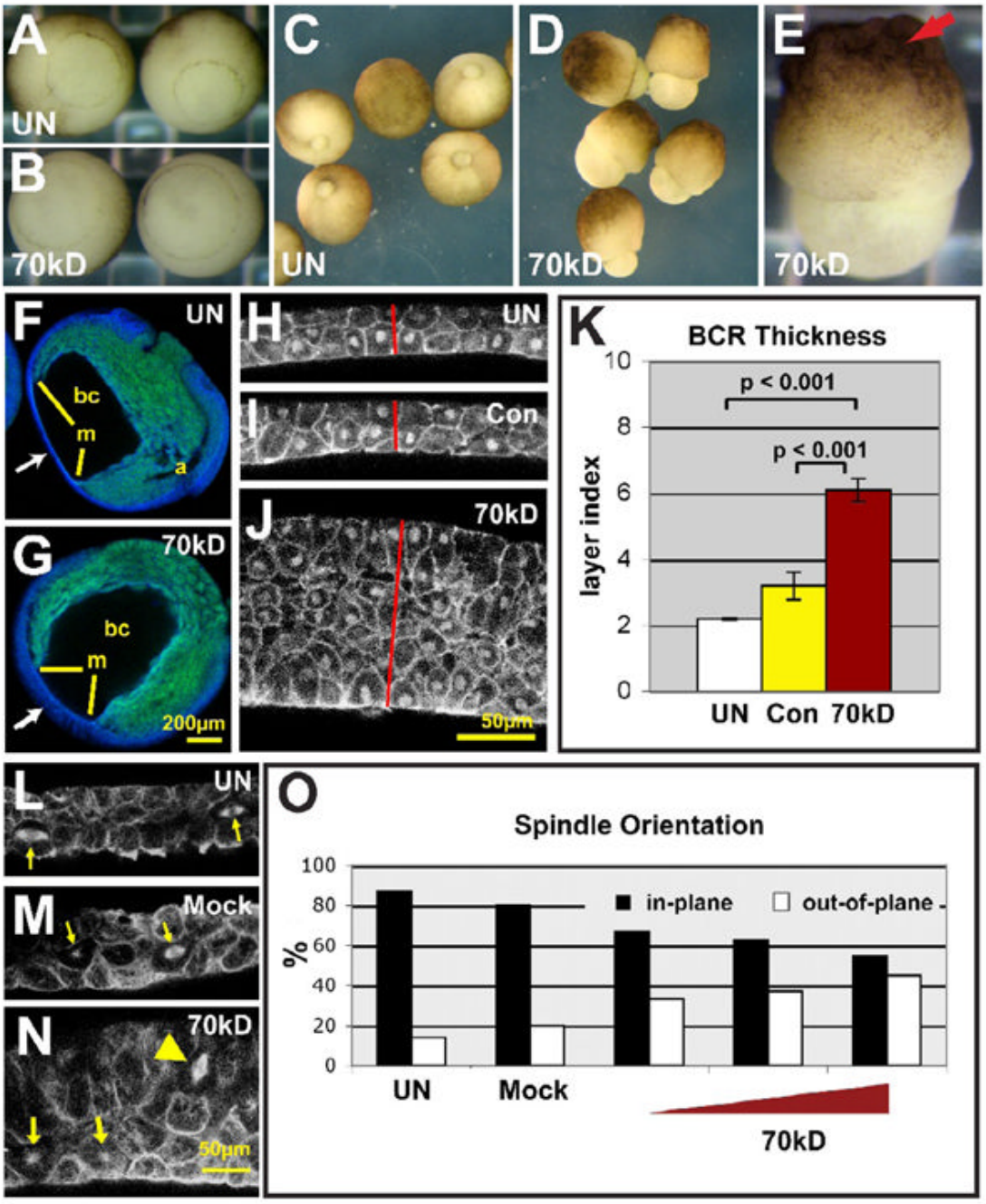

Fig. 6.

70 kD FN blocks epiboly, radial intercalation and randomizes mitotic spindle orientation. (A–E) Vitelline membranes were removed at (A,B) stage 10.5. After 5 hours at 14° C, uninjected gastrulae (C) were normal but 70 kD FN embryos (D) were mushroom shaped. The animal caps of 70 kD FN embryos were bumpy and wrinkled (E, red arrow) indicating that radial intercalation in the BCR was perturbed. (F-G) Confocal micrographs of midline sagitally bisected embryos immunostained for C-Cadherin (blue). Autofluorescence of the yolky endodermal cells appears green. White arrows indicate the BCR (bc, blastocoel; a, archenteron; m, margins of mesendoderm). (H–J) Confocal micrographs of sagitally bisected BCRs immunostained for C-Cadherin. Red lines indicate relative thickness of the BCRs. (K)

Quantification of the average number of cells in the BCR (layer index) from 5 experiments (*n*=2–7 embryos per group). Error bars are ± SEM; results from Student's *t*-tests are indicated. (L–N) Sagitally bisected BCRs immunostained for α-tubulin to visualize mitotic spindles. Yellow arrows: "in-plane" spindles (within 30° of the horizontal plane or single puncta in the center of a cell); yellow arrowhead: "out-of-plane" spindles (within 30° of the vertical plane) (Marsden and DeSimone, 2001). (O) Quantification of spindle orientation from a representative experiment. Red triangle represents increasing expression of 70 kD FN (*n*= 35–160, per group).

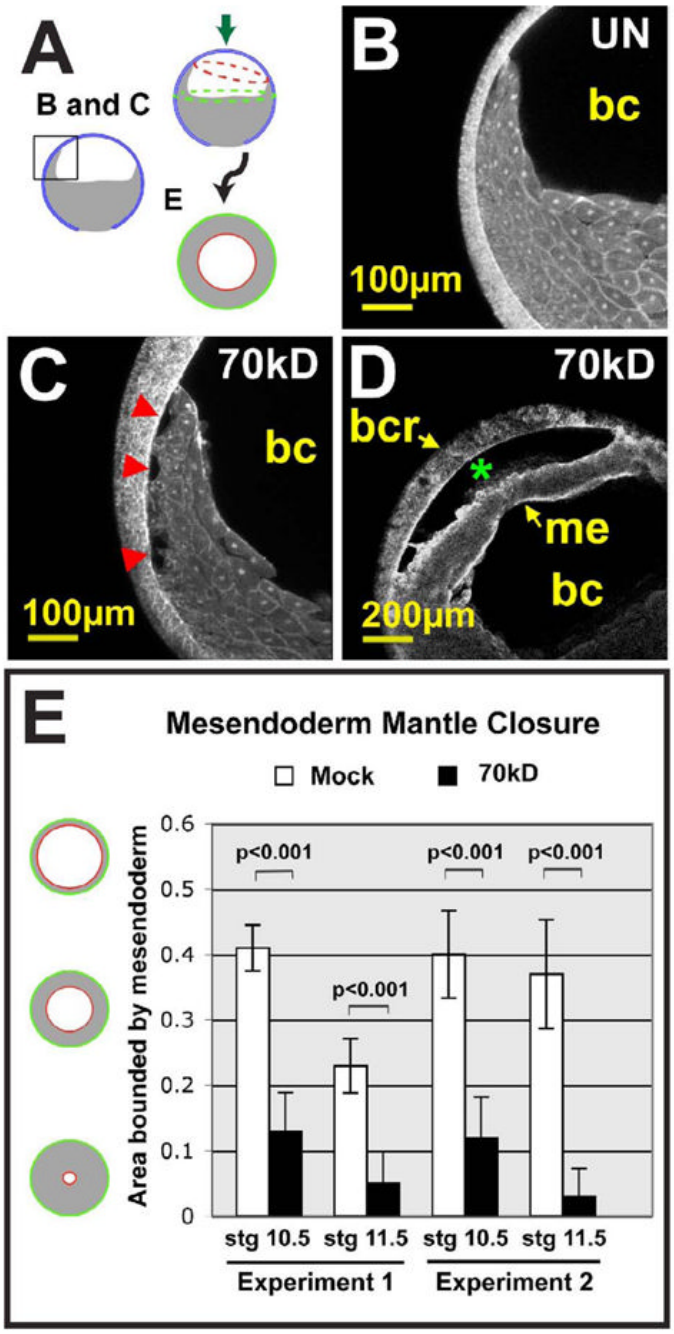

Fig. 7.

Decreased adhesion and accelerated mesendodermal mantle closure accompanies loss of FN Fibrils. (A) Cartoon depiction of the area (black box) imaged in (B) and (C). The dotted ellipses trace the perimeter of the embryo equator (green) and mesendoderm margin (red). When viewed *en face* from the direction of the green arrow, two circles are observed. The ratio of the area bounded by the red circle to the green circle was calculated to represent extent of mesendodermal mantle closure in (E). (B, C) Extended focus confocal z-series of sagitally bisected gastrulae immunostained for C-Cad, through 70–100μm. Embryos are oriented with the animal pole up with partial views of the blastocoel (bc) at upper right. Red arrowheads in (C) indicate gaps between the migrating mesendoderm and the BCR. (D) Sagitally bisected 70

kD FN embryo following fusion of the mesendoderm margins. Green asterisk indicates space between the BCR and the detached mesendoderm (me). (E) Quantification of mesendodermal mantle closure between stg. 10.5 and stg. 11.5 from two independent experiments as illustrated in (A). Ratio of 1 means the mesendodermal mantle is at its maximal open position at the level of the equator and a ratio of 0 means that the mesendoderm margins have fused at the animal pole (i.e. closed position). Significance by *t-test* as indicated. Error bars plot the standard deviations. (Exp 1: n=9–10 and Exp 2: n=4–8 per group).

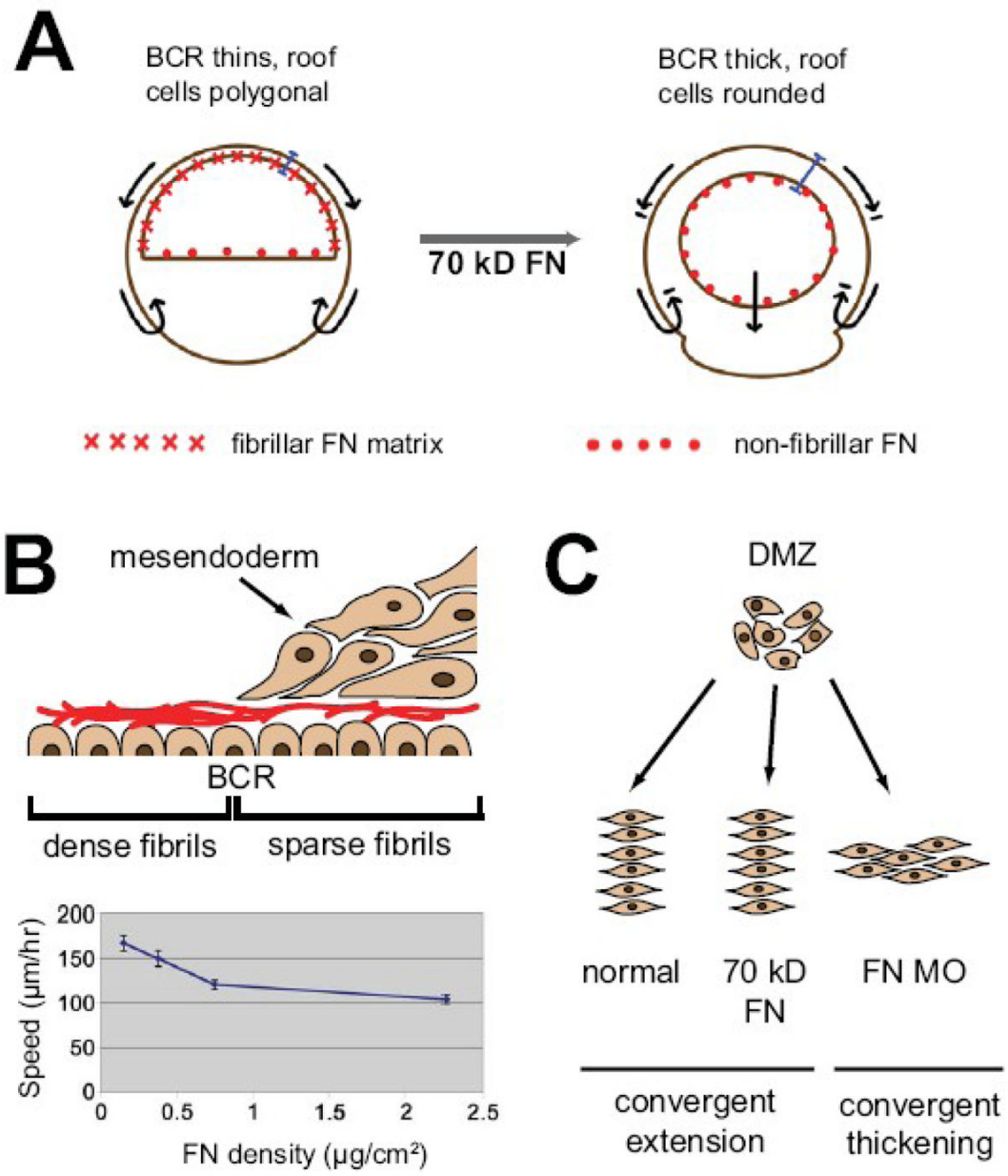

Fig. 8.

Overview of FN fibril functions at gastrulation. (A) Cartoon of 70 kD FN-induced BCR thickening. Direction of normal movements indicated by black arrows; BCR thickness indicated by blue brackets; red crosses represent FN fibrils; red dots represent non-fibrillar FN at cell surfaces. Embryos are oriented animal pole up and vegetal pole down. (B) FN fibrils on normal BCRs are more dense prior to contact with migrating mesendoderm and are more sparsely distributed as the mesendoderm migrates over the BCR (Davidson et al., 2004). Dense fibrils correlate with increased CCBD availability and can inhibit migration by promoting too much cell adhesion. Graph represents the decreasing rate of mesendoderm migration plated on a glass substrate coated with increasing FN density as described in methods. For each density of FN, 36–95 cells were examined from 3–8 experiments. Error bars are ±SEM. (C) Convergent extension in the DMZ requires FN expression, but not assembly into a fibrillar matrix.

Embryo phenotypes following FN fibrillogenesis inhibition

I. Gastrula stage phenotypes

	2 of 2 cells injected			2 of 4 cells injected (DMZ)		
Experiment	**% Normal**	**% Stalled BP closure**	**N[a]**	**% Normal**	**% Stalled BP closure**	**N[a]**
Uninjected	100 ±0	0 ±0	5	100 ±0	0 ±0	3
Mock	100 ±0	0 ±0	2	100 ±0	0 ±0	3
Con RNA	99 ±2	1 ±2	3	nd	nd	0
70kD FN RNA	2 ±3	98 ±3	5	98 ±3	2 ±3	3

II. Tailbud stage phenotypes

	2 of 2 cells injected				2 of 4 cells injected (DMZ)			
Experiment	**% Normal**	**% Short A-P Axis**	**% Failed gastrulation**	**N[a]**	**% Normal**	**% Short A-P Axis**	**% Failed gastrulation**	**N[a]**
Uninjected	95 ±4	3 ±5	0 ±0	4	98 ±1	2 ±1	0 ±0	3
Mock	94 ±6	0 ±0	0 ±0	2	90 ±6	10 ±6	0 ±0	3
Con RNA	96 ±4	2 ±2	0 ±0	2	nd	nd	0 ±0	0
70kD FN RNA	1 ±1	73 ±15	26 ±16	4	93 ±4	7 ±4	0 ±0	3

[a] typical experiment: n = 9–50 embryos per group

± SEM